Influence of Molecular Weight on Self-Organization, Uniaxial Alignment, and Surface Morphology of Hairy-Rodlike Polyfluorene in Thin Films

**Matti Knaapila,*,† Kaisa Kisko,‡ Benjamin P. Lyons,† Roman Stepanyan,§ Joel P. Foreman,†
Oliver H. Seeck,‖ Ulla Vainio,‡ Lars-Olof Pålsson,† Ritva Serimaa,‡ Mika Torkkeli,‡ and
Andrew P. Monkman†**

*Organic Electroactive Materials Research Group, Department of Physics, University of Durham, South Road,
Durham DH1 3LE, United Kingdom, Division of X-ray Physics, Department of Physical Sciences, P.O. Box 64,
FIN-00014, University of Helsinki, Physics of Complex Fluids Group, Department of Applied Physics,
University of Twente, P.O. Box 217, 7500 AE Enschede, The Netherlands, and Institut für Festkörperforschung,
Forschungszentrum Jülich GmbH, D-52425 Jülich, Germany*

We present investigations of the self-organized structure, overall uniaxial alignment, and larger-scale interface morphology in thin films of low-molecular-weight hairy-rodlike π-conjugated poly(9,9-bis(ethylhexyl)-fluorene-2,7-diyl), (LMW-PF2/6) (M_n = 7600 g/mol) and a comparison of high-molecular-weight PF2/6 (HMW-PF2/6) (M_n = 150 000 g/mol). Photoabsorption, grazing-incidence X-ray diffraction, small/wide-angle X-ray scattering, and X-ray reflectivity methods have been used. The experiments have been supported by molecular mechanics-calculated molecular structure and recursively simulated reflectivity curves and discussed in terms of the semiquantitative theoretical analysis of the self-organization of hairy-rodlike polymers. As with HMW-PF2/6, LMW-PF2/6 is found to be a thermotropic liquid crystal consisting of rodlike 5/2 helices. Blue photoluminescence with an absolute photoluminescence quantum yield of 32% in the solid films is observed. After thermotropic alignment on rubbed substrates, considerably higher dichroic ratios in absorption, >10, are found, indicating a far higher degree of axial alignment compared to the similarly processed HMW-PF2/6. The degree of spatial order has been found to be high along the rubbing direction, the **z** axis but, in contrast to HMW-PF2/6, the structure perpendicular to the **z** axis on the (*ab*0) plane is observed to be less ordered, and no multiple orientation (Knaapila, M.; Lyons, B. P.; Kisko, K.; Foreman, J. P.; Vainio, U.; Mihaylova, M.; Seeck, O. H.; Pålsson, L.-O.; Serimaa, R.; Torkkeli, M.; Monkman, A. P. *J. Phys. Chem. B* **2003,** *107,* 12425−12430) is seen. Both in bulk and in thin aligned films, LMW-PF2/6 is suggested to approach a nematic instead of a well-defined hexagonal structure. These findings are in agreement with the presented theoretical arguments. LMW-PF2/6 is also shown to form well-developed larger-scale morphology and surface roughness below 2 nm in films over the thickness range from 20 to 200 nm. There is also a difference in macroscopic texture in polarized micrographs between these materials, but the influence of the molecular weight cannot be rigorously established at present.

1. Introduction

The design of self-organized structures[1] and thin films[2,3] and an understanding of structure−property relationships[4] are key issues in the research of π-conjugated polymers. These polymers are typically s.c. hairy-rodlike materials consisting of a rigid or semirigid backbone where a dense set of side chains is bonded in a comb-shaped manner. (See poly(alkylthiophenes) (PATs)[5,6] as an archetype where hairy-rodlike structure leads to the self-organization with enhanced electronic characteristics.[2,7]) Among π-conjugated hairy rods, polyfluorenes (PFs)[8] have emerged as promising materials for applications. They exhibit thermotropic liquid crystallinity (LC) rendering facile overall alignment that results in the emission of linearly polarized light when used in polarizing light-emitting diodes (LEDs)[9] and enhances mobility when utilized in thin-film transistors (TFT).[10,11] Altogether their

chemical and molecular structure,[8] intermolecular self-organization,[12] overall alignment,[10] larger-scale morphology in films and at interfaces,[13] and thermal behavior[14,15] determine their optoelectronic performance. In accordance with the hierarchy concept of supramolecular chemistry,[16] the structural levels of PFs should also, within the bounds of possibility, be discussed in a concerted manner.[4,8]

Poly(9,9-bis(ethylhexyl)-fluorene-2,7-diyl) (PF2/6)[8] is a particularly interesting PF. PF2/6 is a hole-transporting material with high photoluminescence and electroluminescence quantum yields emitting in the blue region of the spectrum,[17] which can be tuned by energy transfer to dopants.[18] PF2/6 has measurable long-lived electrophosphorescence and delayed electroluminescence at low temperature,[19] and as a side-chain mesomorphic liquid crystal, it can be easily aligned.[20] The structure of PF2/6 has been studied in the solid state using X-ray powder[15] and fiber diffraction[21] (XRD) as well as in in-plane[12] and axially aligned thin films[20,22] using grazing-incidence X-ray diffraction (GIXD). There are also ellipsometric studies on the optical constants−the refractive index and the absorption coefficient−

* Corresponding author. E-mail: matti.knaapila@durham.ac.uk. Tel: +44-191-33-43558. Fax: +44-191-33-43585.
† University of Durham.
‡ University of Helsinki.
§ University of Twente.
‖ Institut für Festkörperforschung.

of uniaxially aligned PF2/6 films[23] and light-scattering and small-angle neutron-scattering studies of PF2/6 solutions.[24] Besides PF2/6, the structure of a related PF polymer, poly(9,9-(di-*n*,*n*-octyl)fluorene) (PF8) has been studied in fibers[25,26] and in films,[27] and optical constants of in-plane-aligned poly(9,9-dioctylfluorene-*co*-benzothiadiazole) (F8BT)[13] are known. PF2/6 and F8BT can be axially highly aligned. In general, PF2/6 has been suggested to attain a higher degree of alignment than PF8.[8]

Recently, Banach et al.[28] have shown for the first time the influence of molecular weight on thermotropically aligned PF, F8BT. These authors used a molecular weight range of $M_n = 62\,000-129\,000$ g/mol and found the highest dichroic ratios in absorption in lowest-molecular-weight films and concluded that the degree of alignment is limited both by viscosity and, in particular, by the formation of an equilibrium (macroscopic) multidomain structure in-plane. On the other hand, we have recently studied the structure and thin-film formation of high-molecular-weight PF2/6 ($M_n = 147\,000$ g/mol, $M_w = 260\,000$ g/mol) (HMW-PF2/6) and found the coexistence of two differently oriented crystalline structures, a multiple orientation in axially *and* in-plane-aligned thin films.[20,22] Somewhat similar orientation phenomena in π-conjugated polymers have previously been found only for stretch-aligned poly(*p*-phenylenevinylene)[29] and in-plane-aligned poly(3-hexylthiophene).[2,3] Besides those, monoaxial distributions (i.e., inverse combs), have been found for PATs.[30]

In this work, we study the film-formation properties of low-molecular-weight ($M_w = 15\,000$ g/mol, $M_n = 7600$ g/mol) PF2/6 (LMW-PF2/6) films using photoabsorption, GIXD, and X-ray reflectivity over a thickness range from 20 to 200 nm. These experiments are supported by bulk XRD and simulations and theoretical considerations. When HMW-PF2/6 was used in our studies, the dichroic ratios in absorption and thus the degrees of uniaxial alignment were not high.[20] In phenomenological consistency with the earlier results with F8BT,[28] we find that when otherwise corresponding processing conditions[20] are employed the low molecular weight of PF2/6 results in a considerably higher degree of axial alignment. In accordance with the earlier[20,21] and parallel[15] studies and the simulation presented here, we suggest that LMW-PF2/6 forms a 5-helix, but unlike the situation with HMW-PF2/6,[20] we do not observe multiple orientations of crystallites. Furthermore, although the axial orientation is much improved; we do not observe considerable local order in the (*ab*0) plane, and the material is less crystalline than HMW-PF2/6 and is suggested to be nematic. This is in clear agreement with the XRD patterns of bulk polymers. On the basis of the underlying theories of hairy-rodlike polymers, we assume this to be related to the fact that we actually approach an oligomeric limit where the transition from hexagonal to nematic structure occurs. Moreover, we show that the surface quality of LMW-PF2/6 films is high and that surface roughness is low up to a film thickness of 40 nm but increases after this. These findings make LMW-PF2/6 an intriguing material for use in aligned PF films and clearly show the importance of molecular-weight-related studies of PF films in general.

2. Theoretical Section

A hairy-rodlike polymer and its self-organized hexagonal and nematic phases are illustrated in Scheme 1. The hairy-rodlike polymers[31] can be discussed using concepts borrowed from the theory of copolymers,[32,33] an approach for which a good experimental resemblance has been found.[34] Real hairy-rods

SCHEME 1: Schematics[a] and Hexagonal Phase[b] of the Hairy-Rodlike Polymer and Uniaxially Aligned[c] and Nematic Polymers[c]
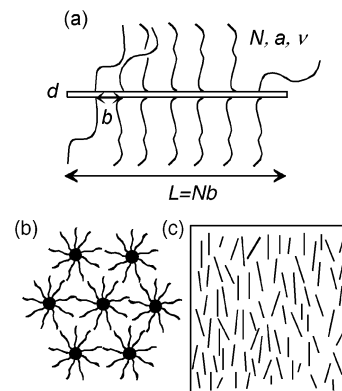
[a] Polymer consists of a stiff backbone and flexible, covalently connected side chains. N, a, and ν are the number of segments, the segment length, and the volume, respectively. b is the distance between grafting points, and L is the length of the rod. [b]Self-organized hexagonal phase of the polymer drawn end-on. [c]Drawn side-on.

such as PF2/6 are not exactly rigid (cf. Fytas et al.[24]). This can be further addressed but is not essential in our phenomenologic consideration. Instead of focusing on the derivation of the free energies, we consider the essence of the physics behind the phenomena, which have been experimentally observed and presented in this paper.

In the transition from nematic to hexagonal phase, the hairy-rodlike molecules lose their translational freedom but reduce the interaction free energy when the molecules are fixed in the lattice positions. We employ a semiquantitative analysis based on the comparison between the free energies of the observed phases. The free energy of the nematic phase has been estimated[33] as

$$F_N \approx k_B TVc \ln f + k_B TVc \ln \frac{4\pi}{\Omega_N} \tag{1}$$

where the translational and orientational entropy are represented by the first and second terms, correspondingly. Here $k_B T$ is a Boltzman factor, V is the volume of the sample, c is the concentration of hairy-rodlike molecules, and f is the volume fraction of the backbone in the molecule. The quantity Ω_N describes the degree of overall (uniaxial) alignment: the smaller it is, the more aligned the obtained system.

The hexagonal phase is characterized by negligibly small translational entropy, and the interaction between hexagonally ordered molecules becomes important. As described for block copolymers, this interaction arises from the inhomogeneous side-chain ends distribution (cf. Semenov[35]). In the case of hairy-rodlike polymers, it is approximately equal to[33]

$$F_{\text{lattice}} \approx k_B TV \frac{\nu}{\nu_0 a^2 b} \tag{2}$$

where ν is the volume, a is the length of one chain segment, b is the distance between two consecutive grafting points, and ν_0 is the volume of one repeat unit of the hairy rod. Considering eq 2, we obtain the free energy of the hexagonally ordered material as

$$F_H \approx k_B TVc \ln \frac{4\pi}{\Omega_H} - k_B TV \frac{\nu}{\nu_0 a^2 b} \tag{3}$$

Influence of Mol Wt in Polyfluorene Thin Films

J. Phys. Chem. B, Vol. 108, No. 30, 2004 **10713**

SCHEME 2: Chemical Structure of Studied Phenylene End-Capped Poly(9,9-bis(ethylhexyl)-2,7-diyl) (PF2/6) and Side View of the Schematics of the Used Multilayers Comprising Aligned PF2/6, Rubbed Polyimide (PI) as an Alignment Layer, and an Indium Tin Oxide (ITO) Layer on the Glass Substrate[a]
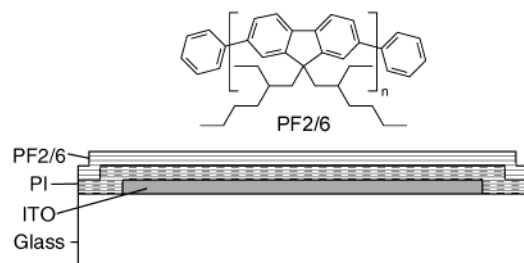
[a] In this work, the degree of polymerization, *n*, is around 20. Thicknesses of PI, ITO, and glass are around 30 nm, 100 nm (measured using X-ray reflectivity), and 1 mm, respectively.

Because of incompressibility, the concentration $c = 1/(v_0 N)$ for the melt is directly related to the molecular weight *M*.

Inspecting eqs 1 and 3, we conclude that the hexagonal packing is more favorable for a high molecular weight. The value of *M* separating nematic and hexagonal phases for given parameters, M^*, is estimated from the comparison of the two free energies and reads as

$$M^* \approx \frac{a^2 b}{v} \ln \frac{1}{f} \qquad (4)$$

In deriving eq 4, we assume both phases to be equally aligned (i.e., $\Omega_N \approx \Omega_H$ in eqs 1 and 3). For a more accurate treatment, we should account for the $F_{lattice}$ temperature dependence due to the enthalpic part of the lattice free energy, which we neglect here. Thus, M^* will change with temperature as well. Equation 4 gives us a qualitative hint and an understanding of the influence of the systems' parameters on the nematic−hexagonal transition.

3. Experimental Section

3.1. Materials and Alignment. The preparation of PF2/6[36,8] (Scheme 2) and oriented PI layers[37] has been described elsewhere. The molecular weight was determined using GPC: HMW-PF2/6: $M_w = 262\,000$ g/mol, $M_n = 147\,000$ g/mol.; LMW-PF2/6: $M_w = 15\,000$ g/mol, $M_n = 7600$ g/mol. For bulk XRD, PF2/6 was used as such. Corresponding to the previously reported preparation of HMW-PF2/6 films,[20] LMW-PF2/6 was dissolved in toluene (Aldrich), and the experimental protocol contained cases I−IV having concentrations of 5, 10, 20, and 40 mg/mL, respectively. Two parallel sample series were made in a clean room by spin coating solutions I−IV onto quartz (Spectrosil quartz disks of Saint-Gobain Quartz Plc) and onto pretreated PI substrates (LCD cells obtained from EHC Ltd., Japan, and split open for this purpose), respectively, at 2500 rpm for 60 s. All of the samples were subsequently annealed under nitrogen at 175 °C for 4 h and cooled at a rate of 3 °C/min. Both the bulk polymer and all samples were stored under nitrogen or helium and/or in the dark or under yellow light to prevent any photooxidation during measurements.

3.2. Optical Measurements. Optical micrographs were taken using an Olympus BX51 microscope equipped with crossed polarizers. Absorption measurements on the unaligned films were made using a Perkin-Elmer Lambda-19 spectrometer. Polarized absorption measurements were made using a JA Woollam & Co. VASE ellipsometer with built-in polarizers,

set up in the transmission mode. A bare PI substrate was used as a reference. The dichroic ratio for absorption is defined as $d = \bar{E}_\parallel / \bar{E}_\perp$, where $\bar{E}_\parallel$ is the maximum value of the absorbance for light polarized parallel to the molecular **c** axis (i.e., the polymer backbone) and $\bar{E}_\perp$ is the maximum value for light polarized perpendicular to it. The dichroic ratio describes the anisotropy of the absorption process. The transition probability is maximized when the transition moment of the molecule lies parallel to the electric vector of the light and the transition moment is assumed to be equal to the **c** axis.

The absolute photoluminescence quantum yield (PLQY) was determined from fresh spin-coated films using a Jobin-Yvon Fluoromax fluorimeter equipped with an integrating sphere and calculated as described in ref 38. The excitation wavelength was 375 nm, corresponding to an excitation maximum.

3.3. X-ray Diffraction and X-ray Reflectivity Measurements. Powder XRD measurements were conducted with a sealed Cu K_α tube using the point focus. The beam was monochromatized with a nickel filter and a totally reflecting glass plate. The beam size was reduced with slits to be 0.1 mm × 0.5 mm on the sample. The scattering distance was 170 mm, and the intensity was measured with a Hi-Star area detector. The *q* ranges were calibrated using a silver behenate standard. Samples were annealed in situ using a Linkham hot stage under a nitrogen atmosphere.

GIXD and X-ray reflectivity measurements were performed at the W1.1 (ROEWI) beam line at HASYLAB in Hamburg, Germany. The beam was monochromatized by a double-crystal Si(111) monochromator, and the X-ray energy was 8.8 keV. The beam was focused on the sample, and the resulting beam size in the experimental hutch was 1.5 mm vertically and 4 mm horizontally. The samples were mounted on the diffractometer by means of two translation axes and a horizontal tilt axis. Scattering by air and the risk of radiation damage were reduced by containing the sample in a helium atmosphere.

In GIXD, the incident angle was 0.09 or 0.11°, selected to cut off Bragg reflections due to the PI substrate. In the measurement geometry, the **x** axis is defined normal to the surface, and **y** and **z** axes are parallel to surface, with **z** coinciding with the rubbing direction of the PI. The GIXD patterns were measured with the incident beam along the **y** and **z** axes, respectively. In reflectivity measurements, the incident angle was equal to the take-off angle. The 1D intensity was measured with a scintillation counter, and 2D intensity was measured with an image plate (Molecular Dynamics); for normalization, the incident flux was measured with an ionization chamber. The Born approximation was regarded as valid except for angles close to the critical angle.[39]

4. Computational Section

4.1. Molecular Modeling. A single molecule of PF2/6 was completely optimized (energy gradients <0.02 kcal/mol) using the conjugate gradient method with the COMPASS force field.[40] The model was created from 10 preoptimized (*R,S*)-*trans*-bifluorene units so that the natural helical twist was maintained. The resulting oligomer of chain length 20 adopts a trans−trans configuration that minimizes the steric interactions between adjacent ethylhexyl side chains. Partial charges were assigned to all atoms using the charge-equilibration scheme,[41] and no symmetry constraints were applied. All calculations were performed using the Discover program within Materials Studio 2.2 from Accelrys Inc.

4.2. X-ray Reflectivity. The reflectivity depends on the material, its thickness, and the surface roughness. Quantitatively,

10714 *J. Phys. Chem. B, Vol. 108, No. 30, 2004*

Knaapila et al.

TABLE 1: Materials Parameters Used in the Modeling of X-ray Reflectivity at 8.8-keV Photon Energy[a]

material	density (g/cm^3)	chemical composition	δ (10^{-6})	β (10^{-6})
quartz	2.65	SiO$_2$	7.11219	0.07959
PF2/6	0.97	C$_{29}$H$_{40}$	2.84700	0.00324

[a] Density of PF2/6 from ref 21.

the reflectivity of a medium j can be described in terms of the refractive index n_j, expressed to a good approximation by

$$n_j = 1 - \delta_j + i\beta_j = 1 - \frac{\lambda^2 \rho_j}{2\pi} + i\frac{\lambda \rho_{\text{abs}_j}}{4\pi} \quad (5)$$

where λ is the wavelength, ρ is the scattering-length density, and ρ_{abs} is the linear absorption coefficient of the given medium. For polymers, δ is on the order of 10^{-6}, and thus the critical angle of total internal reflection, $\alpha_c \approx \sqrt{2\delta}$, is on the order of milliradians. Above the critical angle, the reflectivity decreases rapidly, and thus it plays an important role only at very small angles of incidence in the vicinity of the critical angle.

The intensity reflected by a multilayer was calculated in terms of the layer-by-layer recursive method of Parrat.[42] Air (vacuum) above the multilayer is layer number one, so the layer on top will be layer number 2, the second layer will be number 3, and the substrate number will be $N+1$.[43] At every interface, a part of the incoming beam will be reflected, and the rest is transmitted. Thus, in every layer j there will be a wave transmitted through the interface above (T_j) and a wave reflected by the interface below (R_j). The ratio between the reflected and transmitted amplitudes in layer j is then

$$X_j = \frac{R_j}{T_j} = \exp(-2ik_j z_j)\frac{r_{j,j+1} + X_{j+1}\exp(2ik_{j+1}z_j)}{1 + r_{j,j+1}X_{j+1}\exp(2ik_{j+1}z_j)} \quad (6)$$

where $k_j = (2\pi/\lambda)\sqrt{n_j^2 - \cos^2\alpha_i}$ is the wave vector, α_i is the angle of incidence, $z_{j+1} - z_j$ is the thickness of the layer $j + 1$, and $r_{j,j+1} = (k_j - k_{j+1})/(k_j + k_{j+1})$ is the Fresnel reflectivity for the interface j, $j + 1$. The interfacial roughness between two layers was described using a hyperbolic tangent profile with a rms roughness parameter σ. This leads to small modifications in the Fresnel coefficients.[43] For the start of the fitting procedure, we assumed that the substrate was infinitely thick so that there will be no wave reflected by the interface below it and thus $R_{N+1} = X_{N+1} = 0$. For the air (vacuum) above the multilayer, $T_1 = 1$, and thus the final reflected intensity will be $X_1 = R_1$.[44]

The material parameters used in our calculations are listed in Table 1. The effects of the experimental conditions (i.e. the wavelength, the size of the beam on the sample, and the diffractometer resolution) were also included in our model.

5. Results and Discussion

5.1. Molecular Structure. Figure 1 shows the molecular mechanics-calculated molecular structure of PF2/6 (cf. chemical structure of PF2/6 in Scheme 2). Our present work concerns a single gas-phase molecule of PF2/6 at zero temperature. We note that results presented here are similar to those in our previous work[20] and that of Lieser et al.[21] and Winokur et al.,[15] where significant justification is given for modeling in vacuo. At the molecular level, a single PF2/6 has a helix-forming hairy-rodlike or wormlike architecture (cf. Scheme 1). In Figure 1, the mean optimized interplanar angle between two adjacent fluorene groups of a single oligo-PF2/6 is 144.7°, a value almost

equal to the theoretical ideal for a $^5/_2$ helix (i.e., 5 monomers realize 2 turns). Similar results have been reported in earlier[21] and parallel[15] work, and we have previously reported an oligo-PF2/6 triad for which a somewhat larger angle was observed.[20] However, in that report, we considered an intermolecular hexagonal-like structure consisting of unit cells of three PF2/6 chains. As discussed in section 2, a hexagonal structure is not expected here a priori for a low-molecular-weight hairy rod. Furthermore, in contrast to our previous work, to facilitate the overall uniaxial alignment a small PF2/6 chain of approximately 20 repeat units (LMW-PF2/6) was selected in the experiment. It is worth noting that the molecular weight of the calculated oligo-PF2/6 structure in Figure 1 is the same as that for the experimentally studied LMW-PF2/6. The chirality of the side chains plays a minor role in the gross molecular properties of interest here. Recent work by Winokur et al.[15] shows that the R,R enantiomer has very similar properties.

5.2. Self-Organized Structure. HMW-PF2/6 has previously been shown to form hexagonal self-organized structure in fibers.[21] This is consistent with theory,[32] where a hexagonal structure (Scheme 1b) is generally predicted for rodlike polymers with bulky, branched side chains. There is no structural data for F8BT, but on the basis of XRD, poly(9,9-dioctylfluorene-co-bithiophene) (F8T2)[11] is suggested to be lamellar instead of hexagonal. PF2/6 is simpler than F8BT[28] and F8T2,[11] which are copolymers; therefore, its behavior may be better predicted by theory, where the structure shown in Scheme 1a is assumed.

Figure 2 shows XRD patterns of annealed bulk HMW-PF2/6 and LMW-PF2/6 at room temperature. The crystallite size of PF2/6 has been reported to improve substantially during annealing[15,20] resembling the behavior of F8T2.[11] Figure 2a shows an XRD pattern of HMW-PF2/6 annealed at 180 °C. As expected, HMW-PF2/6 is disordered after synthesis, but the crystallite size becomes significantly larger with the first heating−cooling cycle over the order−disorder transition (ca. 170 °C). Characteristically, very sharp hexagonal patterns with lattice parameter $a = 16.7$ Å appear almost immediately, although further annealing may still improve the structure.[15] Also, a strong 005 reflection always appears at 0.78 Å^{-1}, giving the meridional lattice parameter $c = 40.5$ Å. The positions and integrated intensities of the peaks of HMW-PF2/6 are in agreement with both GIXD[20] and fiber XRD[21] results and more recent powder XRD patterns.[15] These authors report numerous features and conclude PF2/6 to be a 5-helix, most probably a $^5/_2$ helix. In contrast, parts b and c of Figure 2 show XRD patterns of LMW-PF2/6 after annealing at 130 and 180 °C, respectively. In the first curve, there are traces of a hexagonal pattern, but the second curve is more characteristic, showing only one reflection that we recognize to be 005. No distinguished hexagonal patterns are observed when changing the annealing conditions. We interpret this result as evidence that LMW-PF2/6 is significantly less ordered on the (ab0) plane than HMW-PF2/6 and nematic (Scheme 1c) rather than well-defined hexagonal. Still, by analogy to HMW-PF2/6, a prominent reflection at 0.78 Å^{-1} suggests that LMW-PF2/6 takes a helical shape with lattice parameter $c = 39.5$ Å.

The local order of liquid-crystalline polymers may be generally expected to be enhanced with molecular weight.[45] However, the experiment suggests not only the difference in crystallite size but also the transition from the hexagonal to the nematic phase. On the basis of the discussion in section 2, a qualitative interpretation can be given. The free energy of the lattice does not depend on the length of the molecules, which are assumed to be mounted on top of each other to form
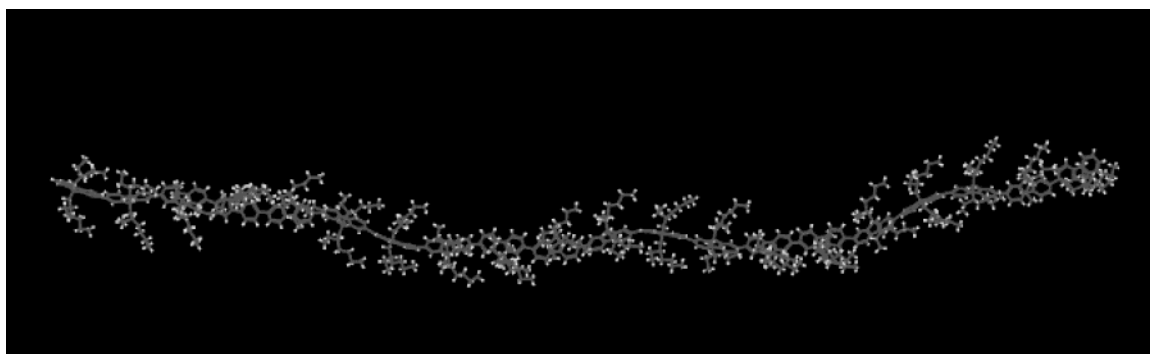
Influence of Mol Wt in Polyfluorene Thin Films

J. Phys. Chem. B, Vol. 108, No. 30, 2004 **10715**

Figure 1. Molecular mechanics-calculated structure of a 20 repeat unit PF2/6 chain. Intramolecular distances are detailed in the text.
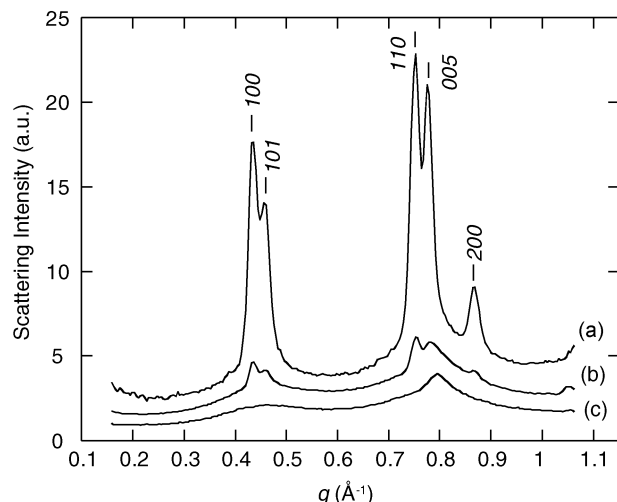

Figure 2. XRD patterns of bulk PF2/6 at room temperature. (a) HMW-PF2/6 after annealing at 180 °C. (b) LMW-PF2/6 after annealing at 130 °C. (c) LMW-PF2/6 after annealing at 180 °C. All samples were annealed for 2 h and cooled at 3 °C/min. Upper curves are shifted for clarity.
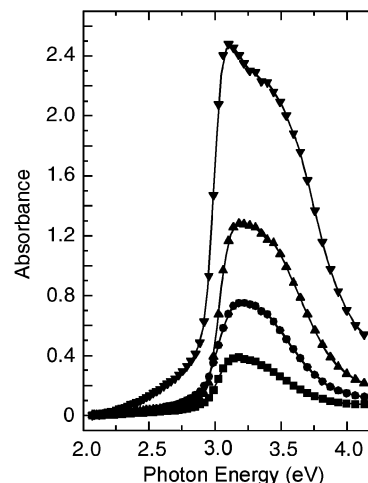

Figure 3. Photoabsorption spectra of LMW-PF2/6 films on quartz. Case I (■), case II (●), case III (▲), and case IV (▼). Data were interpolated by splines.

cylinders, whereas the translational entropy does via concentration. Therefore, for a fixed volume of the sample, if molecules are long and thus concentration is small, then the hexagonal phase wins because the first term in eq 1 approaches zero whereas the second term in eq 3 is negative. Otherwise, the nematic phase is more favorable.

LMW-PF2/6 is rather polydisperse, and it may be asked how this influences the structure. The higher-weight fractions may contribute to the sharpness of the meridional reflection. However, in simple liquid crystals, polydispersity normally leads to a macrophase separation of the long species that form the ordered phase from the short ones in the isotropic phase, and we suggest that the polymer is not seriously macrophase-separated (cf. section 5.5). In such case, we should also observe the coexistence of both features. Figure 2b shows some traces of hexagonal structure that are probably due to higher-molecular-weight fractions. However, as far as we present only a qualitative analysis together with the huge difference in molecular weight between LMW-PF2/6 and HMW-PF2/6, this aspect may be neglected.

5.3. Overall Alignment. The alignment method and protocol used here correspond to our previous work[20] and that used by Lieser et al.[21] making the comparison between the experiments relevant. The alignment procedure broadly corresponds to the conditions needed to achieve high local order in bulk HMW-PF2/6. However, we have also found that lower temperatures and shorter annealing times give almost equal results in overall orientation,[23] and we specifically point out that the same

conditions do not necessarily maximize both the degree of local order and the degree of alignment. In accordance with our previous studies,[20] the molecular axis (the **c** axis) was expected to align along the surface in the rubbing direction, which is parallel to the **z** axis of the GIXD arrangement.

Figure 3 shows the absorption spectra for the LMW-PF2/6 films spun onto quartz. These resemble the usual PF2/6 absorption spectra, but case IV (40 mg/mL film) shows an additional foot and peak that we attribute to scattering due to the thickness of this film. As expected, the films show no polarization dependence in absorption. Instead, as mentioned before, good in-plane orientation has been previously shown.[17]

Plots of the absorption spectra for the aligned LMW-PF2/6 for light polarized perpendicular and parallel to the alignment direction are shown in Figure 4. There are no significant shifts in energy between the films on quartz and those on PI, but in the latter case there indeed is a large difference between the two polarization components, indicating that the films are uniaxially highly aligned. Scattering from the substrate makes it difficult to determine accurate optical densities, but we estimate the films to have absorption dichroic ratios of at least 11.5 ± 2.5, 10.5 ± 1.5, and 9.0 ± 1.5 for increasing film thickness. The data in Figure 4d is somewhat noisy because the thickness of the sample makes accurate measurement difficult, and we may not determine the exact dichroic ratio in absorption. In general, the level of film alignment of LMW-PF2/6 is quite independent of the film thickness within the limits of error. However, the dichroic ratios that we report here show a large improvement over those of HMW-PF2/6 in our previous work.[20] It therefore seems that nematic LMW polymer is far
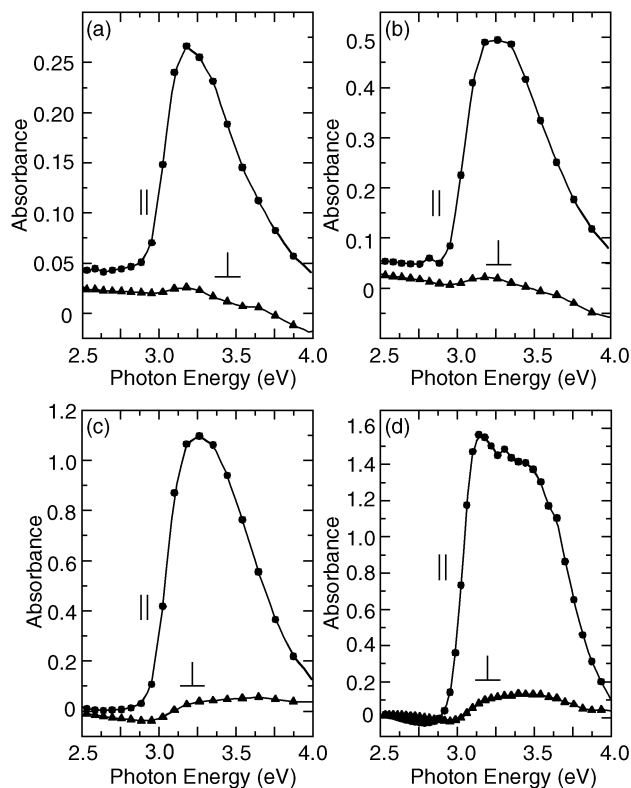
Figure 4. Polarized photoabsorption spectra of uniaxially aligned LMW-PF2/6 films. Subfigures a−d correspond to cases I−IV, respectively. The data were measured using polarized light with the expectation that the **c** axis was parallel (ρ) (●) and perpendicular (σ) (▲) to the polarization vector of the probe light. Data were interpolated by splines.

Figure 5. PL spectrum of LMW-PF2/6 measured in an integrating sphere. Case II on quartz. The excitation wavelength was 375 nm, corresponding to the excitation maximum.

more easily aligned, perhaps because of fewer chain entanglements.

The Ω parameters in eqs 1 and 3 are generally related to the orientational order parameter in the aligned phases, and normally we expect $\Omega_N \geq \Omega_H$ as far as the low-molecular-weight liquid crystals are concerned; the orientational order parameter (for a fixed molecule length) in the vicinity of the transition is about 10% higher in the smectic phase.[46] At first sight, this seems to contradict the experimentally observed better uniaxial alignment of LMW-PF2/6 over that of HMW-PF2/6. However, two explanations can be given. The first one, discussed by Banach et al.,[28] is due to the much larger viscosity of HMW-PF2/6, which does not allow the dichroic ratio to saturate during reasonable observation times. This is a purely kinetic effect. Alternatively, we can turn to the analogy of polymeric liquid crystals. A similar effect, when long persistent molecules align much worse than very short molecules, is known in the theory of nematic ordering in polymer systems described by Khokhlov and Semenov.[47,48] There it is shown that for very short $^{L}/_{\lambda} \ll$ species, where L is the length of molecule and λ is its Kuhn segment, the nematic order parameter can be as high as approximately 0.8, whereas in the regime of long chains it lies around 0.5. The size of the PF2/6 monomer is known from modeling and X-ray diffraction.[21,20] If λ of PF2/6 is further estimated to be around 7 nm[24] and independent of molecular weight, then $^{L}/_{\lambda}$ is around 2 for LMW-PF2/6, whereas for HMW-PF2/6 it is about 80. Despite the absence of quantitative agreement, it is possible that a somewhat similar effect as described in refs 47 and 48 is present in the system under study.

The intra- and intermolecular distances between a few chains play a role in photoexcitations, and the entanglements may affect
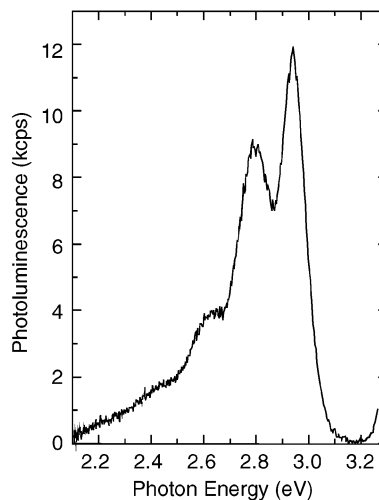
the PLQY, too. In spin-coated films, the studied LMW-PF2/6 shows a similar PL spectrum (Figure 5) to that seen in a high-molecular-weight polymer,[20] and PLQY was measured to be high, approximately 32%. Therefore, the lower molecular weight does not alter the photoluminescence, and 20 units clearly is longer than the effective conjugation length. Furthermore, the increased proportion of chain ends does not seem to increase the number of quenching sites. No major impurities that could result in the quenching of PLQY are expected either.

5.4. Aligned Self-Organized Structure. The predicted features of PF2/6, like those of the hexagonal phase, concern bulk, whereas in films, the surface effects play an additional role. In particular, the hexagons of HMW-PF2/6 are flattened along the surface normal, and the material is observed to reveal two distinct orientation types of self-organized structure, a multiple orientation.[20] Figure 6 shows an example of GIXD patterns of HMW-PF2/6 adapted from ref 22. Figure 6a shows two hexagonal-like patterns, one with a hexagonal axis **a** normal to the surface (cf. black indices in Figure 6a) and another where a hexagonal axis lies in the surface plane (cf. white indices in Figure 6a). These characteristics correspond to the crystallites of orientation types I and II illustrated in Scheme 3. In both cases, the **c** axis is also in the surface plane. In the presented case, the intensity of the pattern of type I is 2.5 times higher than that of type II. Furthermore, the hexagonal lattice parameters in fibers[21] are $a = 16.7$ Å, $c = 40.4$ Å, and $\gamma = 120°$, but in films, we suggested some deviations from the hexagonal phase.[20] The molecular models detailed in section 5.1 indicate that the average distance between an atom in one monomer and the equivalent atom five monomers distant is somewhat larger, 41.6 ± 0.1 Å, whereas the values 40.4 Å[21] and 40.8 Å[15] have been obtained elsewhere.

Figure 7 presents an example of the 2D GIXD patterns of aligned LMW-PF2/6 on PI. All of the samples studied were uniaxially well aligned, as revealed by polarized photoabsorption (Figure 4). Nevertheless, in contrast to HMW-PF2/6 none of them exhibits well-developed hexagonal patterns (cf. Figure 6a and 7a) when treated and measured otherwise similarly. Because we repeated these measurements several times and made them under similar conditions, we may exclude the possibility of experimental error and conclude that the low molecular weight results in considerably less ordered local structure in the (*ab*0) plane in the studied thin films under given circumstances. In particular, unlike some traces in the bulk XRD pattern shown
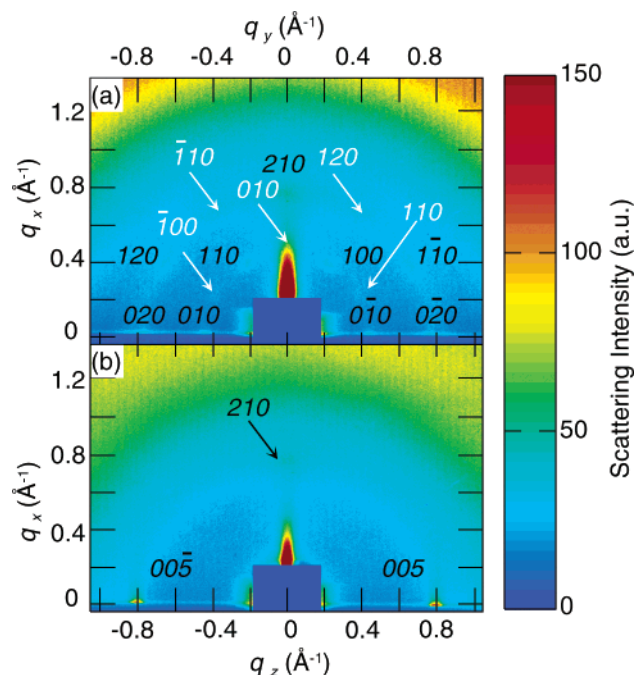
Influence of Mol Wt in Polyfluorene Thin Films

J. Phys. Chem. B, Vol. 108, No. 30, 2004 **10717**

Figure 6. Two-dimensional GIXD patterns of HMW-PF2/6. The film was prepared by spin coating from 2 mg/mL toluene solution and annealing at 175 °C for 3.5 h. (a) (xy0) plane. (b) (x0z) plane. The black indices show primary reflection planes of orientation type I, and white indices show those of type II (cf. ref 20). Reflection 210, which belongs to type I (marked with the black indices), is not in the same plane as reflections −110 and 120, which belong to type II (marked with the white indices). The ratio of the intensities of the types is roughly 2.5. Adapted from ref 22.

SCHEME 3: Mutual Orientation of Orientation Types I and II of HMW-PF2/6 with Respect to the Surface Plane[a]
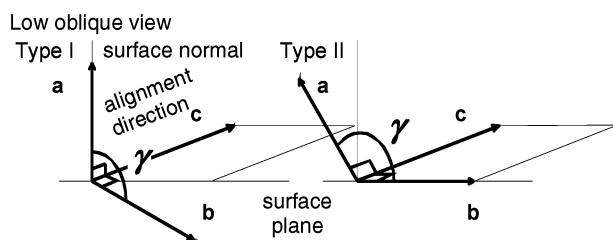
[a] Adapted from ref 22.

in Figure 2b, we cannot resolve hexagonal GIXD patterns at all.

Figure 8 shows 1D axial (out-of-plane and in-plane) GIXD scans of case II of LMW-PF2/6 on PI. A prominent 005 reflection corresponding to the lattice parameter $c = 39.5$ Å is seen in-plane but not out-of-plane indicates high *in-plane* orientation. The total absence of other 00l reflections is explained by the fact that the polymer chains form a very regular $5/_q$ helix and the variation between the bond and toroid angles is small. This is consistent with the result presented in Figure 1 and shows that LMW-PF2/6 forms a well-defined molecular period where the helicity is maintained. Because we do not see other prominent characteristics in 2D data in the (xy0) plane, which indicate locally far less ordered structure than HMW-PF2/6, we assume this to be related to the almost oligomeric character of material that may form a frozen-in nematic phase rather than well-ordered hexagons. Although we kept the incident angle below the critical angle, the penetration depth may still be large, up to 100 Å. PI also shows a 006 reflection at 0.8 Å^{-1} in the GIXD data,[49] near 005 of PF2/6,[21,20] so a
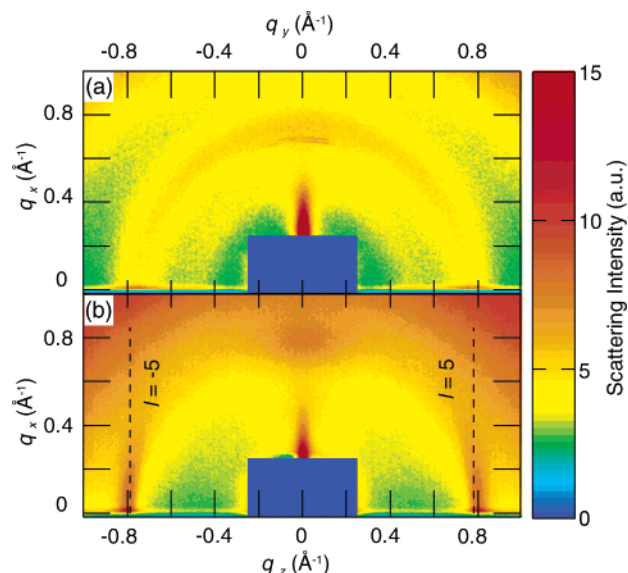

Figure 7. Two-dimensional GIDX patterns of LMW-PF2/6 of case II on rubbed PI when annealing at 175 °C for ca. 4 h were employed. (a) (xy0) plane. The sharp feature at $q_x = 0.7$ Å^{-1}, $q_z = 0$ is due to the substrate. (b) (x0z) plane. The dashed lines show the primary reflection planes. The thickness of the film is around 40 nm.
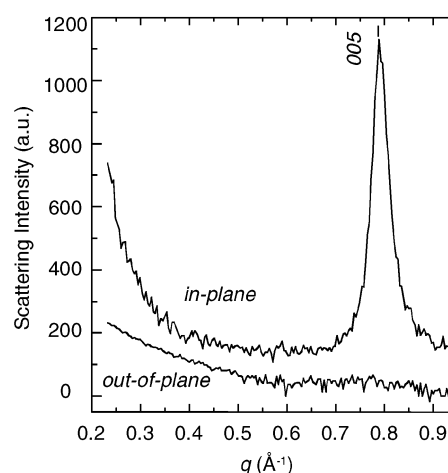

Figure 8. One-dimensional axial (in-plane and out-of-plane) GIXD scans measured along the **y** axis of case II of LMW-PF2/6 on a PI substrate (parallel sample). The prominent 005 reflection seen in-plane but not out-of-plane indicates PF2/6 to be aligned in-plane. The upper curve has been offset for clarity.

possible contribution from PI should be considered. However, because we are not able to resolve other 00l reflections of PI, which should appear, for instance, at 0.4 Å^{-1}, this contribution appears not to be significant here. We also observed a peak at 0.8 Å^{-1} when LMW-PF2/6 was spun on glass.

The local order in hexagonal PF2/6 has been studied extensively by Winokur et al. using powder XRD combined with modeling.[15] These authors found that although the crystallite size may be significantly improved upon annealing (revealed by XRD) the local helical structure of PF2/6 shows only tiny changes (revealed by Raman scattering). However, as seen in the studies of the multiple orientation of π-conjugated polymers,[2,20,29] the structural behavior in powder PF may not completely correspond to that in films. Also, as seen in present work and that of Banach et al.,[28] the nature of PFs may be strongly influenced by parameters such as molecular weight, making the overall picture quite complicated.
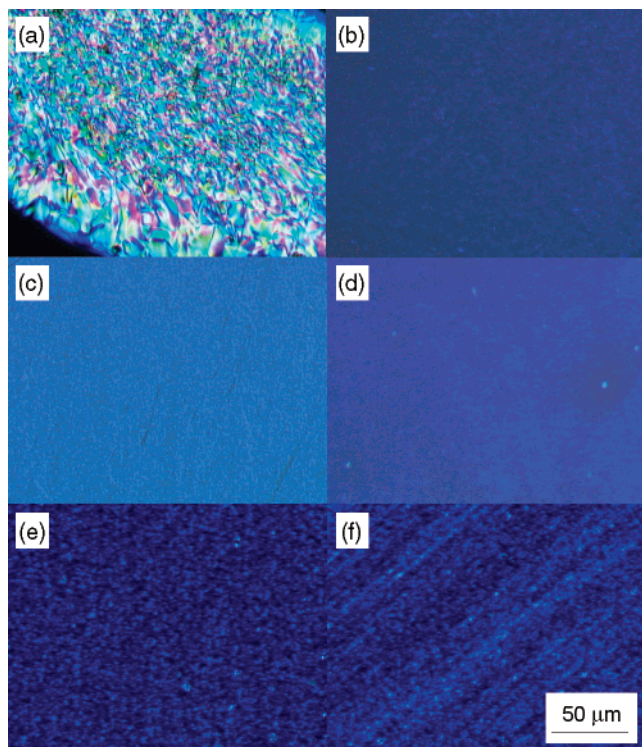
Figure 9. Optical micrographs of PF between crossed polarizers at room temperature. (a) Liquid-crystalline bulk LMW-PF2/6. The black area in the corner is air. (b) LMW-PF2/6 film on quartz spun from a 10 mg/mL solution. (c, d) Aligned LMW-PF2/6 on PI spun from a 20 mg/mL solution and annealed at 80 °C for 10 min observed with the alignment direction parallel and 45° to the first polarizer, respectively. (e, f) HMW-PF2/6 on PI spun from a 10 mg/mL solution and annealed at 175 °C for 2 h observed with the alignment direction parallel and 45° to the first polarizer, respectively.

5.5. Larger-Scale Film Morphology. Besides spatial and orientational ordering, the larger-scale film morphology determines the optoelectronic performance and usefulness of PF thin films. Its relation to the molecular weight of F8BT has been widely studied by Banach et al.[28] Figure 9 presents optical micrographs of the studied PF2/6. PF2/6 is a frozen-in LC at room temperature (Figure 9a) and becomes fluid during heating while remaining birefringent. A characteristic blue birefringent texture is observed under crossed polarizers and is due to the self-organization, not the alignment. When the films were prepared and handled under clean-room conditions, no holes and no major defects in optical resolution were seen in films on quartz (Figure 9b), but those on PI may show a few inhomogeneities if the solution is not filtered.

Parts c, d and e, f of Figures 9 show polarized micrographs of aligned LMW-PF2/6 and HMW-PF2/6 on PI substrate when the alignment direction is parallel or 45° to the first polarizer, respectively. The bright domains are due to imperfectly aligned polymers. The first sample (Figure 9c and d) represents well-aligned nematic-type monodomain structure, but the latter one (Figure 9e and f) reveals less well-aligned hexagonal structure with multiple orientation (cf. Scheme 3). There is a phenomenological difference in the polarized micrographs of these materials. LMW-PF2/6 always forms very uniform films with uniform birefringence in optical resolution down to the micrometer scale. Instead, HMW-PF2/6, which shows a multiple orientation as indicated by GIXD, shows less uniform birefringence than nematic samples. The existence of different types of crystallites is related to the decreased overall alignment of PF2/6, which is in phenomenologic agreement with the results
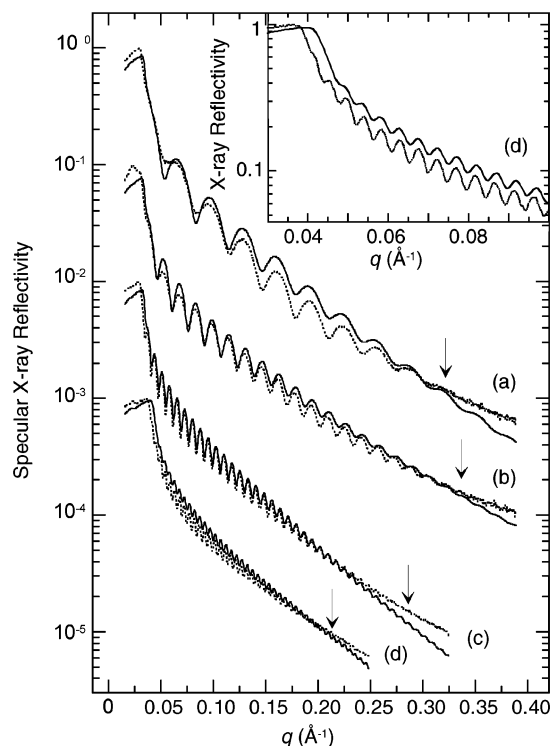

Figure 10. X-ray reflectivity curves of LMW-PF2/6 films aligned in plane on quartz. The calculated curve is represented by solid lines, and the measurement is represented by dotted lines. (a–d) Cases I–IV, respectively. The magnified part of curve of d (case IV) is shown in the inset. The last resolvable fringes are marked with arrows. The reflectivity curves have been shifted relative to each other for clarity.

of *in-plane* multidomains of F8BT as described by Banach et al.[28] Unlike the case for F8BT,[28] we do not find any spherulites for PF2/6 in optical micrographs. We also observed that the multiple orientation in PF2/6 depended on the film thickness,[20] so the crystallites are likely to be distributed out-of-plane rather than in-plane. Because GIXD is not a thickness-sensitive method, we cannot provide a rigorous microscopic explanation of this. However, on the basis of peak broadening the coherence lengths of crystallites of HMW-PF2/6 are on the order of tens of nanometers, thus 2 orders of magnitude lower than the dimensions for domains seen in Figure 9. This means that the observed domains cannot be simply recognized as bare crystallites. There is no significant difference in the degree of orientation between types I and II, but rather the difference is in the (ab0) plane. In conclusion, we are not able to draw the far reaching conclusions that Banach et al.[28] did; they present exceptionally comprehensive optical microscopy work. The question, however, is intriguing because PF films generally show important thickness-dependent features. For instance, the chiro-optical properties of PFs have been shown to depend on the film thickness.[50]

Like optical microscopy, X-ray reflectivity probes large macroscopic areas but sees structural variations down to the nanometer and angström scales. There are very few X-ray reflectivity studies on self-organized π-conjugated materials,[51] and those on PFs seem scarce. Figure 10 shows the X-ray reflectivity of LMW-PF2/6 spun on quartz with the simulated intensities for comparison. The critical angle between PF2/6 and air is found to be around 0.14°. The measurements above the critical angle show the characteristic q^{-4} decay and several oscillations. The period of the oscillations is related to the thickness t of the film (or layer) according to $t \approx {}^{2\pi}/_{\Delta q}$, where Δq is the distance between two successive minima. Accordingly,

Influence of Mol Wt in Polyfluorene Thin Films

J. Phys. Chem. B, Vol. 108, No. 30, 2004 **10719**

TABLE 2: Parameters Fit to the X-ray Reflectivity Data

c (mg/mL)	d (Å)	$\sigma_{quarz/PF2/6}$ (Å)	$\sigma_{PF2/6/air}$ (Å)
5	196 ± 5	8 ± 1	13 ± 1
10	388 ± 5	6 ± 1	13 ± 1
20	812 ± 5	9 ± 1	16 ± 1
40	1795 ± 5	13 ± 1	21 ± 1

the variation in the thickness of the polymer can be clearly seen as a decrease in the period of the oscillation with increasing polymer content. The oscillations fade away after a certain point, which depends on the difference in the roughness of the layers. When the roughnesses are close to each other, the oscillations are resolvable to larger q values. Thus, there seems to be a smaller difference in the roughnesses of the interfaces in cases I−III (5−20 mg/mL) compared to that in case IV (40 mg/mL). This series of last resolvable fringes as a function of film thickness is consistent with our previous study where HMW-PF2/6 was used.[20] We find the quality to depend on the concentration of the mother solution but not very much on the molecular weight of the polymer.

The fitting parameters extracted from the reflectivity data are listed in Table 2. In the simulation, the selected fitting parameters were the thicknesses of the layers and a constant background and roughness of the interfaces, and the materials parameters were held constant. Thus, the only fitting parameter affecting the amplitudes of the oscillations was the roughness. The agreement between the experiment and the model in terms of the period of the oscillations (i.e., the thickness of the polymer layer) is good. The film thicknesses also scale well with the optical density (Figure 3). The amplitudes of the oscillations in the models, however, do not completely correspond to the experimental results, and the listed values are guiding tendencies. However, these results clearly and quantitatively indicate the formation of smooth and well-developed LMW-PF2/6 films. This is in agreement with the AFM results where PFs with branched alkyl side chains are found to form smooth featureless surfaces.[52]

As expected from the earlier results,[53] the Kiessig fringes of the ITO layer dominate the measured reflectivity curves of the multilayers (Scheme 2). The effect of the PF2/6 layers of different thickness is seen on the damping characteristics in the same way as in the case of the quartz substrate (Figure 9). We note, however, that the modeled X-ray reflectivity of multilayers easily gives results that are too different from their expected values to have strict physical significance. Thus, we cannot give reliable quantitative results and conclude that there must be some other, presumably experimental, factors that have not been included in our model. Because the reflectivity measurements are very sensitive to the positioning of the sample, this might be one reason. However, in practice the reflectivity could not be analyzed in more detail because PI and ITO layers did not cover the whole glass substrate (cf. Scheme 2).

6. Conclusions

An experimental study of the film formation of LMW-PF2/6 has been presented for a film thickness range of 20 to 200 nm parallel to computational and theoretical considerations. A low molecular weight was selected, but it was still found to be high enough to provide as efficient a photoluminescence as HMW-PF2/6. However, compared to HMW-PF2/6, a considerably higher dichroic ratio in absorption and thus a higher degree of axial alignment was achieved under similar processing conditions. This phenomenologically confirms the result of Banach et al.,[28] where, however, the oligomeric limit was not ap-

proached. The local order of LMW-PF2/6 on the (*ab0*) plane is much lower than that of HMW-PF2/6 and frozen-in nematics rather than well-ordered hexagonal phases are observed. This is interpreted in terms of the theory of hairy-rodlike polymers and is also explained by analogy to known phenomena in liquid crystals. Moreover, the observed small surface roughness of PF2/6 shows that the quality of the film is high and decreases slightly when increasing the thickness up to around 40 nm. There is a difference in macroscopic texture in polarized micrographs between nematic and multiply oriented hexagonal samples, but the X-ray reflectivity characteristics are not suggested to depend on the molecular weight of PF2/6.

Although further optimization and quantitative theoretical analysis are required to exploit the observations in PF2/6 thin films fully, we conclude that the particular orientation procedure and conditions and materials parameters, such as molecular weight, determine the degree of alignment, and we find that the molecular weight is directly related to the spatial ordering and the multiple orientation of PF2/6. These results form important prerequisite information when preparing thin films of thermotropically aligned PF2/6 for applications or fundamental research. The findings also indicate that the theoretical analysis of hairy-rodlike molecules may be used to predict the experimental results in thin films on rubbed alignment substrates, a system routinely used in molecular electronics. Because PF2/6 belongs to the archetypes of hairy-rodlike polymers, the observations may give guidelines to other alkyl-substituted polyfluorenes, too.

References and Notes

(1) Winokur, M. J. Structural Studies of Conducting Polymers. In *Handbook of Conducting Polymers*; Skotheim, T. A., Elsenbaumer, R. L., Reynolds, J. R., Eds.; Marcel Dekker: New York, 1998; pp 707−726.

(2) Sirringhaus, H.; Brown, P. J.; Friend, R. H.; Nielsen, M. M.; Bechgaard, K.; Langeveld-Voss, B. M. W.; Spiering, A. J. H.; Janssen, R. A. J.; Meijer, E. W.; Herwig, P.; de Leeuw, D. M. *Nature* **1999**, *401*, 685−688.

(3) Aasmundtveit, K. E.; Samuelsen, E. J.; Guldstein, M.; Steinsland, C.; Flornes, O.; Fagermo, C.; Seeberg, T. M.; Pettersson, L. A. A.; Inganäs, O.; Feidenhans'l, R.; Ferrer, S. *Macromolecules* **2000**, *33*, 3120−3127.

(4) Winokur, M. J.; Chunwachirasiri, W. *J. Polym. Sci., Part B: Polym. Phys.* **2003**, *41*, 2630−2648.

(5) Winokur, M. J.; Spiegel, D.; Kim, Y.; Hotta, S.; Heeger, A. J. *Synth. Met.* **1989**, *28*, C419−C426.

(6) Samuelsen, E. J.; Mårdalen, J. The Structure of Polythiophenes. In *Handbook of Organic Conductive Molecules and Polymers*; Nalwa, H. S., Ed.; Wiley: New York, 1997; Vol. 3, pp 87−120.

(7) Sirringhaus, H.; Tessler, N.; Friend, R. H. *Science* **1998**, *280*, 1741−1744.

(8) Scherf, U.; List, E. J. W. *Adv. Mater.* **2002**, *14*, 477−487.

(9) Grell, M.; Bradley, D. D. C. *Adv. Mater.* **1999**, *11*, 895−905.

(10) Sirringhaus, H.; Wilson, R. J.; Friend, R. H.; Inbasekaran, M.; Wu, W.; Woo, E. P.; Grell, M.; Bradley, D. D. C. *Appl. Phys. Lett.* **2000**, *77*, 406−408.

(11) Kinder, L.; Kanicki, J.; Swensen, J.; Petroff, P. *Proc. SPIE-Int. Soc. Opt. Eng.* **2003**, *5217*, 35−42.

(12) Kawana, S.; Durrell, M.; Lu, J.; MacDonald, J. E.; Grell, M.; Bradley, D. D. C.; Jukes, P. C.; Jones, R. A. L.; Bennett, S. L. *Polymer* **2002**, *43*, 1907−1913.

(13) Ramsdale, C. M.; Greenham, N. C. *J. Phys. D: Appl. Phys.* **2003**, *36*, L29−L34.

(14) Cheun, H.; Tanto, B.; Chunwaschirasiri, W.; Larson, B.; Winokur, M. J. *Appl. Phys. Lett.* **2004**, *84*, 22−24.

(15) Tanto, B.; Guha, S.; Martin, C. M.; Scherf, U.; Winokur, M. J. *Macromolecules*, submitted for publication, 2004.

(16) Fyfe, M. C. T.; Stoddart, J. F. *Acc. Chem. Res.* **1997**, *30*, 393−401.

(17) Tammer, M.; Higgins, R. W. T.; Monkman, A. P. *J. Appl. Phys.* **2002**, *91*, 4010−4013.

(18) Lyons, B. P.; Wong, K. S.; Monkman, A. P. *J. Chem. Phys.* **2003**, *118*, 4707−4711.

(19) Sinha, S.; Rothe, C.; Güntner, R.; Scherf, U.; Monkman, A. P. *Phys. Rev. Lett.* **2003**, *90*, 127402(1)−127402(4).

(20) Knaapila, M.; Lyons, B. P.; Kisko, K.; Foreman, J. P.; Vainio, U.; Mihaylova, M.; Seeck, O. H.; Pålsson, L.-O.; Serimaa, R.; Torkkeli, M.; Monkman, A. P. *J. Phys. Chem. B* **2003**, *107*, 12425−12430.

(21) Lieser, G.; Oda, M.; Miteva, T.; Meisel, A.; Nothofer, H.-G.; Scherf, U.; Neher, D. *Macromolecules* **2000**, *33*, 4490−4495.

(22) Knaapila, M. Self-Organized Supramolecules of pi-Conjugated Rodlike Polymers. Doctoral Thesis in Science of Technology, Helsinki University of Technology (Department of Engineering Physics and Mathematics), Espoo, Finland, 2004.

(23) Lyons, B. P.; Monkman, A. P. *J. Appl. Phys.*, submitted for publication, 2004.

(24) Fytas, G.; Nothofer, H. G.; Scherf, U.; Vlassopoulos, D.; Meier, G. *Macromolecules* **2002**, *35*, 481−488.

(25) Grell, M.; Bradley, D. D. C.; Ungar, G.; Hill, J.; Whitehead, K. S. *Macromolecules* **1999**, *32*, 5810−5817.

(26) Grell, M.; Bradley, D. D. C.; Inbasekaran, M.; Ungar, G.; Whitehead, K. S.; Woo, E. P. *Synth. Met.* **2000**, *111−112*, 579−581.

(27) Winokur, M. J.; Slinker, J.; Huber, D. L. *Phys. Rev. B* **2003**, *67*, 184106/1−184106/11.

(28) Banach, M. J.; Friend, R. H.; Sirringhaus, H. *Macromolecules* **2003**, *36*, 2838−2844.

(29) Chen, D.; Winokur, M. J.; Masse, M. A.; Karasz, F. E. *Polymer* **1992**, *33*, 3116−3122.

(30) Prosa, T. J.; Winokur, M. J.; Moulton, J.; Smith, P.; Heeger, A. J. *Macromolecules* **1992**, *25*, 4364−4372.

(31) Wegner, G. *Macromol. Chem. Phys.* **2003**, *204*, 347−357.

(32) Stepanyan, R.; Subbotin, A.; Knaapila, M.; Ikkala, O.; ten Brinke, G. *Macromolecules* **2003**, *36*, 3758−3763.

(33) Subbotin, A.; Stepanyan, R.; Knaapila, M.; Ikkala, O.; ten Brinke, G. *Eur. Phys. J. E* **2003**, *12*, 333−345.

(34) Knaapila, M.; Stepanyan, R.; Horsburgh, L. E.; Monkman, A. P.; Serimaa, R.; Ikkala, O.; Subbotin, A.; Torkkeli, M.; ten Brinke, G. *J. Phys. Chem. B* **2003**, *107*, 14199−14203.

(35) Semenov, A. N. *Sov. Phys. JETP* **1985**, *61*, 733−742.

(36) Grell, M.; Knoll, W.; Lupo, D.; Meisel, A.; Miteva, T.; Neher, D.; Nothofer, H.-G.; Scherf, U.; Yasuda, A. *Adv. Mater.* **1999**, *11*, 671−675.

(37) Lupo, D.; Yasuda, A.; Grell, M.; Neher, D.; Miteva, T. Polyimide Layer Comprising Functional Material, Device Employing the Polyimide Layer, Manufacturing the Device. European Patent Application EP1011154, 2000, pp 1−29.

(38) Pålsson, L.-O.; Monkman, A. P. *Adv. Mater.* **2002**, *14*, 757−758.

(39) Dosch, H. In *Critical Phenomena at Surfaces and Interfaces: Evanescent X-ray and Neutron Scattering*; Hoehler, G., Ed.; Springer Tracts in Modern Physics, Vol. 126; Springer-Verlag: Berlin, 1992.

(40) Sun, H. *J. Phys. Chem. B* **1998**, *102*, 7338−7364.

(41) Rappe, A. K.; Goddard, W. A. *J. Phys. Chem.* **1991**, *95*, 3358−3363.

(42) Parrat, L. G. *Phys. Rev.* **1954**, *95*, 359−369.

(43) Tolan, M. X-ray *Scattering from Soft-Matter Thin Films: Materials Science and Basic Research*; Springer-Verlag: Berlin, 1999.

(44) Seeck, O. H.; Kaendler, I. D.; Tolan, M.; Shin, K.; Rafailovich, M. H.; Sokolov, J.; Kolb, R. *Appl. Phys. Lett.* **2000**, *76*, 2713−2715.

(45) Donald, A. M.; Windle, A. H. *Liquid Crystalline Polymers*; Cambridge University Press: Cambridge, U.K., 1992.

(46) McMillan, W. L. *Phys. Rev. A* **1971**, *4*, 1238−1246.

(47) Khokhlov, A. R.; Semenov, A. N. *Physica A* **1982**, *112*, 605−614.

(48) Khokhlov, A. R. Theories Based on the Onsager approach. In *Liquid Crystallinity in Polymers*; Ciferri, A., Ed.; VCH Publishers: New York, 1991; pp 97−129.

(49) Factor, B. J.; Russell, T. P.; Toney, M. F. *Phys. Rev. Lett.* **1991**, *66*, 1181−1184.

(50) Craig, M. R.; Jonkheijm, P.; Meskers, S. C. J.; Schenning, A. P. H. J.; Meijer, E. W. *Adv. Mater.* **2003**, *15*, 1435−1438.

(51) Tarabia, M.; Hong, H.; Davidov, D.; Kirstein, S.; Steitz, R.; Neumann, R.; Avny, Y. *J. Appl. Phys.* **1998**, *83*, 725−732.

(52) Surin, M.; Hennebicq, E.; Ego, C.; Marsitzky, D.; Grimsdale, A. C.; Müllen, K.; Brédas, J.-L.; Lazzaroni, R.; Leclère, P. *Chem. Mater.* **2004**, *16*, 994−1001.

(53) Clarke, J.; Pape, I.; Normile, P.; Tanner, B. K. *J. Phys. D: Appl. Phys.* **2003**, *36*, A209−A213.